Impurity-induced transition to a Mott insulator in $Sr_3Ru_2O_7$

R. Mathieu,[1,*] A. Asamitsu,[1,2] Y. Kaneko,[1] J. P. He,[1] X. Z. Yu,[1] R. Kumai,[3] Y. Onose,[1] N. Takeshita,[3] T. Arima,[1,4] H. Takagi,[3,5,6] and Y. Tokura[1,3,7]

[1]*Spin Superstructure Project (ERATO-SSS), JST, AIST Central 4, Tsukuba 305-8562, Japan*

[2]*Cryogenic Research Center (CRC), University of Tokyo, Bunkyo-ku, Tokyo 113-0032, Japan*

[3]*Correlated Electron Research Center (CERC), AIST Central 4, Tsukuba 305-8562, Japan*

[4]*Institute of Multidisciplinary Research for Advanced Materials, Tohoku University, Sendai 980-8577, Japan*

[5]*Department of Advanced Materials Science, University of Tokyo, Kashiwa 277-8581, Japan*

[6]*CREST, Japan Science and Technology Corporation (JST)*

[7]*Department of Applied Physics, University of Tokyo, Tokyo 113-8656, Japan*

(Received 28 April 2005; revised manuscript received 21 July 2005; published 8 September 2005)

The electrical, magnetic, and structural properties of $Sr_3(Ru_{1-x}Mn_x)_2O_7$ ($0 \leqslant x \leqslant 0.2$) are investigated. The parent compound $Sr_3Ru_2O_7$ is a paramagnetic metal, critically close to magnetic order. We have found that, with a Ru-site doping by only a few percent of Mn, the ground state is switched from a paramagnetic metal to an antiferromagnetic insulator. Optical conductivity measurements show the opening of a gap as large as 0.1 eV, indicating that the metal-to-insulator transition is driven by the electron correlation. The complex low-temperature antiferromagnetic spin arrangement, reminiscent of those observed in some nickelates and manganites, suggests a long-range orbital order.

DOI: 10.1103/PhysRevB.72.092404 PACS number(s): 74.70.Pq, 71.27.+a, 71.30.+h

The Ruddelson-Popper-type $Sr_{n+1}Ru_nO_{3n+1}$ series shows metallic properties, as well as exotic superconductivity and spin-orbital order. $SrRuO_3$ ($n=\infty$, perovskite) and $Sr_4Ru_3O_{10}$ ($n=3$) are itinerant ferromagnets with Curie temperatures (T_c) around 160 K and 100 K, respectively.[1,2] In contrast, single-layered Sr_2RuO_4 ($n=1$) and double-layered $Sr_3Ru_2O_7$ ($n=2$) do not show ferromagnetism (FM). Sr_2RuO_4 is a well-known superconductor, which displays the unconventional spin-triplet pairing.[3] $Sr_3Ru_2O_7(Ru^{4+}, 4d^4)$ is essentially paramagnetic,[4] although there is some controversy in the literature related to the presence of ferromagnetic $SrRuO_3$ and $Sr_4Ru_3O_{10}$ impurities. A metamagnetic transition is observed at low temperatures in large magnetic fields,[5,6] indicating the presence of quantum criticality. Another signature of this phase competition is found in hydrostatic pressure experiments[8] or Sr-site doping by Ca (Ref. 7) of $Sr_3Ru_2O_7$, which stabilizes the antiferromagnetic (AFM) state. In the case of $Ca_3Ru_2O_7$, which has a lattice structure closely related to that of $Sr_3Ru_2O_7$, the AFM ordering is observed at low temperature ($\sim$56 K). The system remains metallic below this temperature, but near 48 K, a first-order-like transition to a less conductive state is observed.[9]

In this article, we investigate the effects of the Ru-site doping by Mn of $Sr_3Ru_2O_7$. A metal-to-insulator transition is observed as the Mn content increases. Optical conductivity measurements reveal the opening of a Mott-like gap.[10] Neutron diffraction experiments show that the low-temperature insulating state is associated with a novel antiferromagnetic spin arrangement, which suggests some complex orbital order. Interestingly, while there are many observations of insulator-to-metal transitions upon tuning of the one-electron bandwidth or band filling by doping,[11] there are few reports of the opposite—i.e., of the formation of a Mott-like insulating state upon the addition of impurities in a metal. One example of such impurity doping effects is found in the Mott insulator V_2O_3. As V^{3+} is replaced by $Ti^{3+/4+}$, the system becomes metallic by modification of the band filling and/or bandwidth.[12] However, the replacement of V^{3+} by Cr^{3+} instead strengthens the electron correlation (via modification of the lattice and hence the bandwidth), so that the metal-to-insulator transition occurs at higher temperatures than in the undoped compound.[12] In the present case of $Sr_3(Ru_{1-x}Mn_x)_2O_7$, the effect of the impurity doping is even more dramatic. A few percent of Mn yields a drastic phase change, turning the paramagnetic metal $Sr_3Ru_2O_7(x=0)$ into an antiferromagnetic Mott insulator ($x>0.025$).

Single crystals of $Sr_3(Ru_{1-x}Mn_x)_2O_7$ ($x=0$, 0.005, 0.025, 0.05, 0.075, 0.1, and 0.2) were grown by the floating zone method. The Mn composition x was checked by inductively coupled plasma (ICP) analysis. x-ray diffraction and superconducting quantum interference device (SQUID) magnetometry reveal minor impurities of Sr_2RuO_4 and traces of the ferromagnetic $Sr_4Ru_3O_{10}$. The crystals easily cleave along shiny *ab* planes. The in-plane resistivity ρ of the crystals was measured as a function of the temperature T using a standard four-probe method on a PPMS6000 system. The heat capacity was recorded using a relaxation method from $T=0.6$ K to 100 K with the same measurement system. X-ray and neutron diffraction data were collected at selected temperatures with setups using closed-cycle helium refrigerators, for the crystal with $x=0.05$: The x-ray data were recorded on a Rigaku SPD curved imaging plate system by using Si(111)-double-crystal monochromated synchrotron radiation x rays ($\lambda=0.688$ Å) at the beamline BL-1A of the Photon Factory, High-Energy Accelerator Research Organization (KEK), Japan. The cell parameters were calculated from the diffraction peaks of the x-ray oscillation photographs of the single crystal assuming a tetragonal ($I4/mmm$) symmetry in the whole temperature region.

The powder neutron diffraction patterns were collected using a time-of-flight (TOF) diffractometer Vega, KEK, Ja-

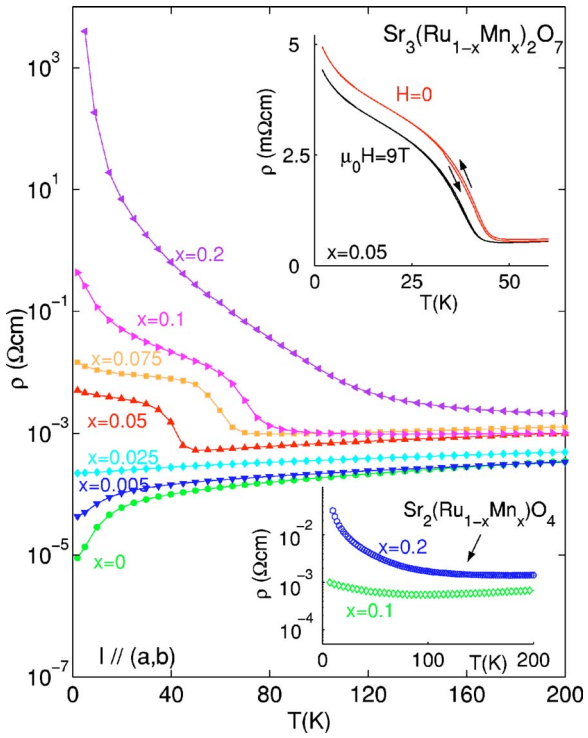

FIG. 1. (Color online) Temperature T dependence of the resistivity ρ of $Sr_3(Ru_{1-x}Mn_x)_2O_7$ for different Mn doping x. The electrical current was fed in the ab plane, and in the experiments shown in the upper inset, a magnetic field of $\mu_0 H=9$ T was applied along the c axis of the crystal with $x=0.05$. The resistivity was recorded on cooling and heating, as indicated by the arrows. The lower inset shows the weaker effect of such a substitution in the case of single crystals of $Sr_2(Ru_{1-x}Mn_x)O_4$ (from Ref. 17) for comparison; this effect is as well weak in the case of $Sr(Ru_{1-x}Mn_x)O_3$ (see Ref. 18) for similar amounts of Mn.

pan. The single crystal was pulverized for this purpose. The obtained powders were sealed with helium gas in a vanadium cell with a diameter of 9.2 mm. TOF diffraction patterns for a wide d range (1–20Å) were obtained at a 30° scattering bank. The optical conductivity spectra $\sigma(\omega)$ of the crystal with $x=0.1$ were measured at different temperatures. Near-normal-incidence reflectivity spectra $R(\omega)$ were collected in the 0.05–3 eV energy range. Kramers-Kronig analysis was performed to derive $\sigma(\omega)$ from the measured $R(\omega)$.

The dramatic effect of the Mn doping on the electrical properties of $Sr_3(Ru_{1-x}Mn_x)_2O_7$ is shown in Fig. 1. While all the samples are metallic at room temperature, only the crystals with $x \leqslant 0.025$ remain metallic at low temperatures. In the low-temperature metallic regime, the residual resistivity increases with x, indicating that Mn impurities act as scatterers. The crystals with $x>0.025$ in contrast show a sharp increase in resistivity at low temperatures. These resistivity jumps are accompanied by an insulating behavior at lower temperatures. The resistivity is discernibly affected by the application of a magnetic field, as seen in the upper inset for $x=0.05$. The resistivity increase due to the metal-insulator transition is shifted to lower temperature with an applied magnetic field. This suggests the antiferromagnetic nature of the lower-lying insulating state.

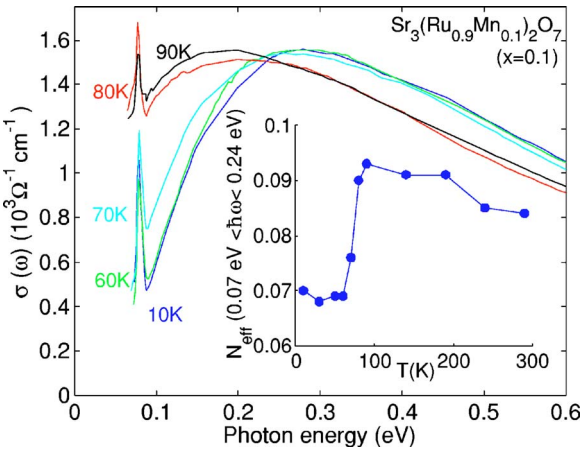

FIG. 2. (Color online) Optical conductivity $\sigma(\omega)$ of $Sr_3(Ru_{0.9}Mn_{0.1})_2O_7(x=0.1)$ at selected temperatures. The sharp peaks near 0.08 eV correspond to optical phonons coupled with the electronic excitations. The inset shows the low-energy spectral weight N_{eff} (effective number of electrons) plotted as a function of the temperature, obtained by integration of $\sigma(\omega)$ between 0.07 eV and 0.24 eV.

The optical conductivity $\sigma(\omega)$ spectra are shown in Fig. 2 for the crystal with $x=0.1$ at different temperatures. Above $T=80$ K, the optical conductivity spectra show a broad peak in the midinfrared region (~0.2 eV), which is typical of the incoherent metallic state[11] in the vicinity of the Mott transition.[10] While $\sigma(\omega)$ shows a minimal temperature variation above 80 K, the spectral weight in the low-energy region is steeply suppressed below $T=70$ K, forming a gaplike structure. As a measure of the spectral weight, we utilize the effective number of electrons, defined as $N_{\text{eff}}(\omega) = (2m_0)/(\pi e^2 N)\int_0^{\omega}\sigma(\omega')d\omega'$,[11] where m_0 is the free-electron mass and N is the number of Ru ions per unit volume. The different $\sigma(\omega)$ curves shown in Fig. 2 define an isosbestic point (equal-absorption point, across which the spectral weights are transferred) near 0.24 eV, the typical energy scale of the Mott gap.[11] Thus, by integrating $\sigma(\omega)$ in the $0.07\ \text{eV} < \hbar\omega < 0.24$ eV energy range, we could estimate the low-energy spectral weight as $N_{\text{eff}}(0.07\ \text{eV} < \hbar\omega < 0.24\ \text{eV}) = N_{\text{eff}}(0.24\ \text{eV}) - N_{\text{eff}}(0.07\ \text{eV})$. As seen in the temperature variation of $N_{\text{eff}}(0.07\ \text{eV} < \hbar\omega < 0.24\ \text{eV})$ shown in the inset of Fig. 2, the formation of a gap occurs between $T=60$ and 80 K, in the vicinity of the resistivity-jump temperature (near $T=78$ K for the crystal with $x=0.1$; see Fig. 1). The Mn impurities increase the disorder. However, this large energy-scale (~0.2 eV) gap formation cannot be explained by disorder-induced localization effects,[13] as the typical energy scale of the Anderson localization is much smaller ($<10^{-2}$ eV). It is worth noting that such a large energy gap formation is observed in the optical spectra of Ca_2RuO_4 (Ref. 14) and other Mott insulators (Ref. 11).

We now investigate the magnetic and structural properties of the insulating state of the crystals with $x \geqslant 0.05$. We display in Fig. 3 the temperature dependence of various physical properties of the system. The low-temperature heat capacity C data of the crystals with $x \geqslant 0.05$ (plotted as C/T) shown in the upper panel and inset of Fig. 3 could be fitted

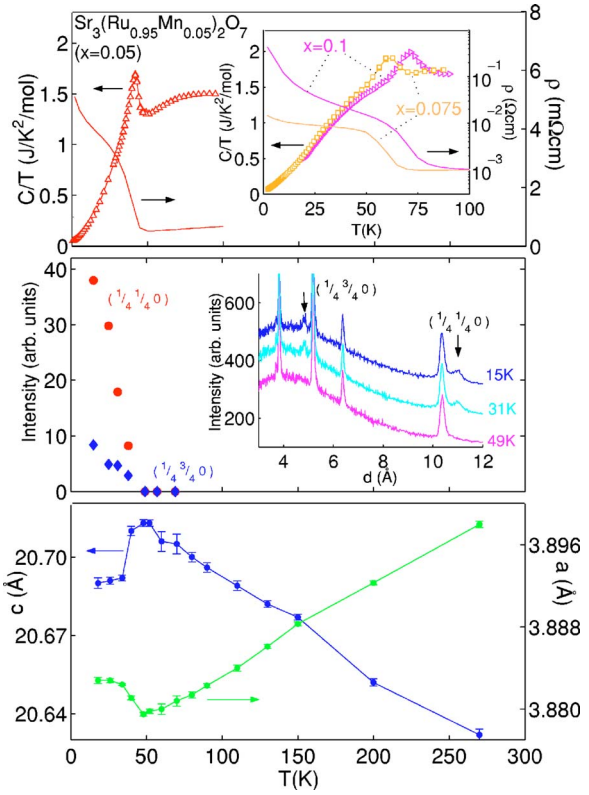

FIG. 3. (Color online) Temperature dependence of different physical properties of $Sr_3(Ru_{0.95}Mn_{0.05})_2O_7(x=0.05)$. Upper panel: heat capacity C plotted as C/T (left axis); the resistivity (ρ) data from Fig. 1 are added for comparison (right axis). The inset of this panel shows the corresponding data for the crystals with $x=0.075$ and $x=0.1$. Middle panel: intensity of the (1/4,1/4,0) and (1/4, 3/4,0) magnetic peaks observed in neutron diffractograms, as shown in the inset. Lower panel: tetragonal a- and c-axis lattice parameters obtained from x-ray diffraction.

with the contributions of conduction electrons (the T-linear coefficient γ shows a weak sample dependence and amounts to 50 ± 5 mJ/mol/K^2) and phonon modes (the T^3-linear coefficient $\beta\sim1\pm0.2$ mJ/mol/K^4). The fit is slightly improved introducing a T^2-linear contribution, which may reflect a magnetic contribution to the heat capacity. More importantly, for the crystals with $x=0.05$ (main frame) and $x>0.05$ (inset), a peak is observed in the heat capacity in the vicinity of the resistivity-jump temperature. In comparison, the heat capacity of the undoped compound (which remains a metal down to the lowest temperature) shows no anomaly.[6] By integrating the data of the Mn-doped crystals after subtraction of a certain base line, an entropy change associated with the transition $\Delta S\sim0.45\pm0.05$ R could be estimated, implying the relevance of the spin entropy. This is confirmed by neutron diffraction experiments. As shown in the middle panel of Fig. 3, the magnetic peaks corresponding to AFM ordering show up below the metal-to-insulator transition temperature.

Furthermore, x-ray diffraction measurements show that around the same temperature the c-axis lattice parameter decreases, as seen in the lower panel of Fig. 3 for $x=0.05$. This may indicate that the RuO_6 octahedra are compressed along the c axis, in a Jahn-Teller-like fashion, or that buckling of

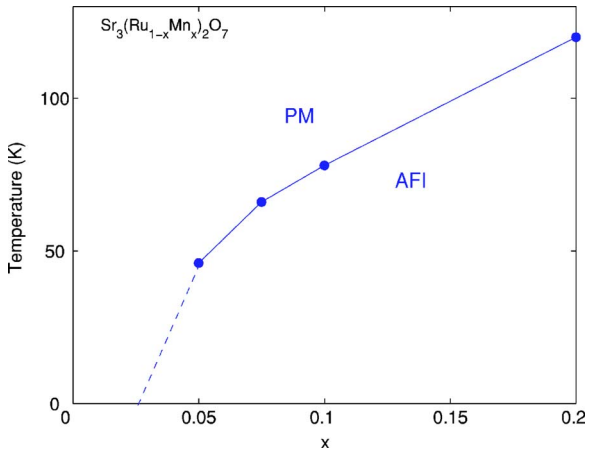

FIG. 4. (Color online) Electronic phase diagram showing the phase boundary between the paramagnetic metal (PM) and antiferromagnetic insulator (AFI) regions. The boundary is plotted using transport data from Fig. 1.

the octahedra occurs. The electrical and magnetic properties of ruthenates are usually associated with the $4d$ orbitals of Ru and their hybridization with the $2p$ orbitals of oxygen. In $Sr_3(Ru_{1-x}Mn_x)_2O_7$, Ru^{4+} is in the $S=1$ low-spin state, so that the e_g levels are empty, and only the t_{2g} orbitals d_{xy}, d_{yz}, and d_{zx} are partially filled. Structural modifications such as distortions of the RuO_6 octahedra yield changes in the relative energy of the t_{2g} orbitals[15] and, hence, in the magnetic interaction. The high-temperature metallic state of $Ca_3Ru_2O_7$ was related to the predominant role of the d_{xy} orbitals.[9] The low-temperature insulating state was then associated with the increased contribution of the d_{yz} and d_{zx} orbitals promoted by lattice changes. However, the contraction of the c axis observed by x-ray diffraction in $Ca_3Ru_2O_7$ (Ref. 16) and in our $Sr_3(Ru_{1-x}Mn_x)_2O_7$ (cf. Fig. 3) amounts merely to $\sim0.1\%$, which is one order of magnitude lower than observed in systems with ferroic d_{xy} orbital ordering such as Ca_2RuO_4.[14]

The measurement of the temperature dependence of various physical properties of $Sr_3(Ru_{1-x}Mn_x)_2O_7$ enables us to draw the schematic electronic phase diagram shown in Fig. 4, which defines the phase boundary between the paramagnetic metal (PM) and the antiferromagnetic insulator (AFI). Antiferromagnetic peaks appear in neutron diffractograms at the metal-to-insulator transition temperatures [no additional peaks appear in the high-Q region or (n/2 1/4 0) peaks]. The most probable magnetic arrangement in the ab plane is an up-up-down-down arrangement (with spins in the ab plane or parallel to the c axis) with the magnetic wave vector of (1/4 1/4 0), although this has to be confirmed by a thorough diffraction study. This spin arrangement is reminiscent of the zigzag chains of the E-type structure[19] observed at low temperatures in manganites with significant $GdFeO_3$-type distortion such as $HoMnO_3$ (Ref. 20), as well as in (Nd/Pr)NiO_3 (Ref. 21) nickelates. In $RMnO_3$ (R being a rare-earth ion), the amount of $GdFeO_3$-type distortion determines the strength of the superexchange interaction between Mn next-nearest neighbors. For small R ions, like Ho, the large superexchange interaction, coupled to the orbital order, yields the spin frustration[20] and the appearance of the E-type

antiferromagnetic state. Hence the complex magnetic structure of $Sr_3(Ru_{1-x}Mn_x)_2O_7$ with $x>0.025$ may reflect some long-range order in the orbital sector.[21,22] The c-axis contraction observed in the vicinity of the resistivity jump is similar to that observed in $Ca_3Ru_2O_7$, as well as in $Ca_{2-x}Sr_xRuO_4$ ($0.2<x<0.5$, so-called "phase II"),[23] which displays a complex orbital order. However, the low-temperature insulating AFM state of $Sr_3(Ru_{1-x}Mn_x)_2O_7(x\geq 0.05)$ does not result from such structural distortions as in the less conductive and two-dimensional metallic state of $Ca_3Ru_2O_7$ or Ca-rich $(Sr,Ca)_3Ru_2O_7$,[16] but from local modification of the orbital states induced by the Mn impurities.

In summary, the physical properties of single crystals of the $Sr_3(Ru_{1-x}Mn_x)_2O_7(0\leq x\leq 0.2)$ system have been investigated. A metal-to-insulator transition, associated with the formation of a large charge gap ($\sim$0.1 eV), is observed as the Mn concentration x increases. The closely correlated temperature dependence of various physical quantities suggests a tight coupling of the lattice, orbital, and spin degrees of freedom. Interestingly, the low-temperature insulating state shows a complex antiferromagnetic spin structure, which suggests some long-range order in the t_{2g} orbital sector. The results illustrate how the impurity doping (substituting only a few percent of Ru) allows phase control of the multicritical layered ruthenates.

We thank Professor T. Ishigaki and Professor T. Kamiyama for their help with the neutron diffraction measurements.

*Permanent address: Cryogenic Center, University of Tokyo, Tokyo 113-0032, Japan. Electronic address: roland@crc.u-tokyo.ac.jp

[1] A. Callaghan, C. W. Moller, and R. Ward, Inorg. Chem. **5**, 1572 (1966).
[2] M. K. Crawford, R. L. Harlow, W. Marshall, Z. Li, G. Cao, R. L. Lindstrom, Q. Huang, and J. W. Lynn, Phys. Rev. B **65**, 214412 (2002).
[3] Y. Maeno, H. Hashimoto, K. Yoshida, S. Nishizaki, T. Fujita, J. G. Bednorz, and F. Lichtenberg, Nature (London) **372**, 532 (1994).
[4] S.-I. Ikeda, Y. Maeno, S. Nakatsuji, M. Kosaka, and Y. Uwatoko, Phys. Rev. B **62**, R6089 (2000).
[5] S. A. Grigera, R. S. Perry, A. J. Schofield, M. Chiao, S. R. Julian, G. G. Lonzarich, S. I. Ikeda, Y. Maeno, A. J. Millis, and A. P. Mackenzie, Science **294**, 329 (2001).
[6] Z. X. Zhou, S. McCall, C. S. Alexander, J. E. Crow, P. Schlottmann, A. Bianchi, C. Capan, R. Movshovich, K. H. Kim, M. Jaime, N. Harrison, M. K. Haas, R. J. Cava, and G. Cao, Phys. Rev. B **69**, 140409(R) (2004).
[7] G. Cao, S. C. McCall, J. E. Crow, and R. P. Guertin, Phys. Rev. B **56**, 5387 (1997).
[8] Y. V. Sushko, B. DeHarak, G. Cao, G. Shaw, D. K. Powell, and J. W. Brill, Solid State Commun. **130**, 341 (2004).
[9] Y. Yoshida, I. Nagai, S.-I. Ikeda, N. Shirakawa, M. Kosaka, and N. Mori, Phys. Rev. B **69**, 220411(R) (2004).
[10] N. F. Mott, Proc. Phys. Soc., London, Sect. A **62**, 416 (1949); *Metal-Insulator Transitions* (Taylor & Francis, London, 1974).
[11] M. Imada, A. Fujimori, and Y. Tokura, Rev. Mod. Phys. **70**, 1039 (1998).
[12] D. B. McWhan, J. P. Remeika, T. M. Rice, W. F. Brinkman, J. P. Maita, and A. Menth, Phys. Rev. Lett. **27**, 941 (1971).
[13] P. W. Anderson, Phys. Rev. **109**, 1492 (1958).
[14] J. H. Jung, Z. Fang, J. P. He, Y. Kaneko, Y. Okimoto, and Y. Tokura, Phys. Rev. Lett. **91**, 056403 (2003).
[15] Z. Fang and K. Terakura, Phys. Rev. B **64**, 020509(R) (2001).
[16] E. Ohmichi, Y. Yoshida, S. I. Ikeda, N. Shirakawa, and T. Osada, Phys. Rev. B **70**, 104414 (2004).
[17] K. Hatsuda, M.Sc. thesis, University of Tokyo, 2001.
[18] G. Cao, S. Chikara, X. N. Lin, E. Elhami, V. Durairaj, and P. Schlottmann, Phys. Rev. B **71**, 035104 (2005).
[19] T. Hotta, M. Moraghebi, A. Feiguin, A. Moreo, S. Yunoki, and E. Dagotto, Phys. Rev. Lett. **90**, 247203 (2003).
[20] T. Kimura, S. Ishihara, H. Shintani, T. Arima, K. T. Takahashi, K. Ishizaka, and Y. Tokura, Phys. Rev. B **68**, 060403(R) (2003).
[21] J. L. Garcia-Munoz, J. Rodriguez-Carvajal, and P. Lacorre, Phys. Rev. B **50**, 978 (1994).
[22] T. Hotta and E. Dagotto, Phys. Rev. Lett. **88**, 017201 (2002).
[23] M. Kriener, P. Steffens, J. Baier, O. Schumann, T. Zabel, T. Lorenz, O. Friedt, R. Mueller, A. Gukasov, P. Radaelli, P. Reutler, A. Revcolevschi, S. Nakatsuji, Y. Maeno, and M. Braden, cond-mat/0408015 (unpublished).